Journal of CO2 Utilization 54 (2021) 101767

Contents lists available at ScienceDirect

Journal of CO2 Utilization

journal homepage: www.elsevier.com/locate/jcou

Effect of N_2 on CO_2-CH_4 conversion in a gliding arc plasmatron: Can this major component in industrial emissions improve the energy efficiency?

Senne Van Alphen [a,b,1,*], Joachim Slaets [a,1], Sara Ceulemans [a], Maryam Aghaei [a], Rony Snyders [b,c], Annemie Bogaerts [a]

[a] Research Group PLASMANT, Department of Chemistry, University of Antwerp, Universiteitsplein 1, 2610, Antwerp, Belgium
[b] Research Group ChIPS, Department of Chemistry, University of Mons, 20, Place du parc, 7000, Mons, Belgium
[c] Materia Nova Research Center, 3 Avenue Nicolas Copernic, 7000, Mons, Belgium

ARTICLE INFO

Keywords:
Plasma-based CO_2-CH_4 conversion
Effect of N_2
Plasma chemistry
Computational modelling
Gliding arc plasmatron

ABSTRACT

Plasma-based CO_2 and CH_4 conversion is gaining increasing interest, and a great portion of research is dedicated to adapting the process to actual industrial conditions. In an industrial context, the process needs to be able to process N_2 admixtures, since most industrial gas emissions contain significant amounts of N_2, and gas separations are financially costly. In this paper we therefore investigate the effect of N_2 on the CO_2 and CH_4 conversion in a gliding arc plasmatron reactor. The addition of 20 % N_2 reduces the energy cost of the conversion process by 21 % compared to a pure CO_2/CH_4 mixture, from 2.9 down to 2.2 eV/molec (or from 11.5 to 8.7 kJ/L), yielding a CO_2 and CH_4 (absolute) conversion of 28.6 and 35.9 % and an energy efficiency of 58 %. These results are among the best reported in literature for plasma-based DRM, demonstrating the benefits of N_2 present in the mix. Compared to DRM results in different plasma reactor types, a low energy cost was achieved. To understand the underlying mechanisms of N_2 addition, we developed a combination of four different computational models, which reveal that the beneficial effect of N_2 addition is attributed to (i) a rise in the electron density (increasing the plasma conductivity, and therefore reducing the plasma power needed to sustain the plasma, which reduces the energy cost), as well as (ii) a rise in the gas temperature, which accelerates the CO_2 and CH_4 conversion reactions.

1. Introduction

In the past decades, it has become clear that global warming represents a severe threat to our current society. Indeed, the climate changes that are caused by enhanced greenhouse gas (GHG) concentrations in the Earth's atmosphere are considered one of the main challenges for the 21 st century [1]. This motivates major research efforts to convert GHG's like CO_2 and CH_4 into value-added chemicals and renewable fuels, thereby closing the so-called "carbon loop". This conversion fits perfectly within the concept of 'cradle-to-cradle', i.e. upcycling waste products into new sustainable feedstock [2].

Several different technologies are being investigated for chemical conversion of CO_2 and CH_4, such as thermo-, photo-, electro- or biochemical conversion, mostly in combination with catalysis [3–7]. Another process that is gaining increasing interest for the conversion of GHG's is plasma technology, as it harmonizes greatly with a future of renewable electricity [3,8]. In plasma-based conversion applications, electric energy is used to activate CO_2 and CH_4 molecules, so that they undergo chemical reactions that would otherwise be thermodynamically unfavoured, like the conversion of CO_2 and CH_4 into CO and H_2, which is called the "dry reforming of methane" (DRM):

$$CO_2 + CH_4 \rightarrow 2CO + 2H_2 \ \Delta H^\circ = 247\ kJ\ mol^{-1} \quad (1)$$

Plasma technology is inherently flexible, being a so-called "turnkey" process, which can easily be switched on and off, following the intermittent energy supply of renewable energy from wind and solar cells. Plasma technology thus delivers the compelling possibility to convert intermittent renewable electricity into fuels and chemicals, which are much more easily storable energy resources or feedstock for the chemical industry. Furthermore, the technology is easily scalable in size and applicability, has a low investment and operating cost, and does not rely on rare earth materials, which may be a limiting factor for other

* Corresponding author at: Research Group PLASMANT, Department of Chemistry, University of Antwerp, Universiteitsplein 1, 2610, Antwerp, Belgium.
E-mail address: senne.vanalphen@uantwerpen.be (S. Van Alphen).
[1] Shared first author.

https://doi.org/10.1016/j.jcou.2021.101767
Received 4 June 2021; Received in revised form 13 October 2021; Accepted 14 October 2021

emerging technologies, like electrochemical and photochemical conversion of CO_2 and CH_4 [3,8].

Plasma is an ionized gas, achieved in its simplest form by applying an electric potential difference between two electrodes, positioned in a gas. The applied electric power selectively heats the electrons in the plasma, which collide with the gas molecules, causing excitation, ionization and dissociation of these molecules. The excited molecules, ions and radicals that are formed in the plasma quickly react further, creating a highly reactive environment capable of breaking down stable molecules like CO_2 and CH_4 [9]. The combined CO_2 and CH_4 conversion allows for the direct plasma-based production of syngas (CO/H_2) by DRM, as well as the formation of oxygenates and higher hydrocarbons [10]. As energy is predominantly transferred to the electrons (typically reaching energies of a few eV, i.e., several 10 000 K), no pre-heating of the bulk gas is needed for the conversion process. The gas itself is intrinsically heated by the plasma reactions, reaching temperatures up to a few 1000 K for gliding arc (GA) reactors, which allows for thermal conversion to occur in addition to the plasma-based conversion. This gives plasma technology a potential edge over thermal conversion of CO_2 and CH_4 in terms of energy effiency [3,9].

Plasma-based DRM has been studied in different types of plasma reactors, leading to very promising results [3,10–18]. The best results are obtained in GA plasmas, showing conversions in the range of 30–50 % with energy costs as low as 1−3 eV [12,18–20]. The very best results were reported for a rotating GA reactor co-driven by a magnetic field, yielding a total conversion up to 40 % at an energy costs of 1 eV/molec [12]. Many of these GA reactors thus meet the efficiency target of 4.27 eV/molec, that was calculated by Snoeckx and Bogaerts [3] based on the required syngas formation to be competitive with other renewable gas conversion and energy storage technologies.

Some studies also explored the addition of N_2 to CO_2 or CO_2-CH_4 plasmas, either to create a more stable plasma or to mimic realistic emissions from industrial plants [21–25]. Vice versa, CH_4 addition to CO_2/N_2 plasma has also been shown to have beneficial effects, like suppressing NO_x formation [26]. Most industrial gas emissions contain significant amounts of N_2, and separation is financially costly [27]. The addition of N_2 thus creates a more realistic situation for the industrial application of plasma-based DRM [28]. For this purpose, more insight is needed in the effect of N_2 on the plasma chemistry and the performance of plasma-based DRM. While adding N_2 inevitably leads to electric power being wasted into excitation, ionization and dissociation of N_2, it has already been demonstrated for pure CO_2 conversion that N_2 assists the CO_2 splitting process [22,24,25], raising the question if N_2 could also be a useful admixture for DRM.

In the present paper we investigate the effect of N_2 on plasma-based DRM and we optimize the N_2 content in the gas feed to achieve maximal performance for a gliding arc plasmatron (GAP) reactor. This novel type of gliding arc reactor was developed at Drexel University by Nunnally et al. [29] to overcome the non-uniform gas treatment of a classical two-dimensional (2D) gliding arc. The GAP has already delivered promising results for pure CO_2 splitting [30], as well as for DRM in CO_2-CH_4 [16] and CO_2-CH_4-O_2 [21] mixtures. In the latter case, N_2 was also present, but in large amounts (60–80 %) to create a more stable plasma, and the focus was on the effect of O_2 addition, while the effect of N_2 on the chemistry and performance was not investigated. N_2 addition to pure CO_2 plasma showed promising results [25], but the effect of N_2 addition for DRM in the GAP has not been studied yet. Therefore, we focus here on optimizing the performance of the GAP for DRM in a wide range of N_2 fractions. We present an in-depth study, both by experiments and computational models. Experimentally we evaluate the energy cost, energy efficiency, the conversion of CO_2 and CH_4, and the product yields and selectivities in the GAP for N_2 fractions ranging from 80 % to 0 %, in which the CO_2:CH_4 ratio is kept at 1:1, as this was found to be the optimal ratio in our previous study [21]. In addition, we combine four different computational models, i.e., a 3D turbulent gas flow model, a 3D thermal plasma model, particle tracing simulations and a quasi-1D plasma chemical kinetics model, to simulate the gas flow, plasma dynamics and plasma chemistry, for the same conditions as the experiments, using the experimental input gas mixture, plasma power, and reactor geometry as input. This novel and sophisticated modelling approach allows us to explain the experimental results and provide insight in both the physical and chemical effects of varying the N_2 fraction in the plasma.

2. Experimental details

The experimental setup consists of three main parts, the reactor, the electric circuit, and the gas analysis system. The gas flow of the different inlet gasses (i.e. CO_2, CH_4 and N_2) is regulated by mass flow controllers (MFC) (Bronkhorst), that are controlled by a computer. These gasses mix in the inlet tube leading to the reactor and enter the reactor through six tangential inlets, of which two are depicted in Fig. 1. This creates an initial vortex flow in the reactor body (at cathode potential) that moves upwards along the reactor walls (yellow arrow in Fig. 1). At the top of the reactor the vortex reverses and turns inwards (blue arrow in Fig. 1) moving the gas downwards to the outlet (at anode potential), after which the gas is transported to a gas chromatograph (GC) (Thermo Scientific trace 1310 GC) with a thermal conductivity detector for gas analysis. The plasma arc first ignites at the shortest distance between the cathode and anode, but is carried by the gas flow to the centre of the reactor, and at steady state it forms a long arc between the top of the reactor (cathode) and outlet (anode), as depicted in red in Fig. 1. In the ideal case, the gas in the inner vortex all moves through the arc, although in reality the arc is typically not wide enough to cover the whole inner vortex flow. The outer gas vortex causes thermal insulation between the hot plasma arc and reactor walls.

The power supply (Advanced Plasma Solutions, PA, USA) is connected to the electrodes. The electrical current is controlled and held at 0.3 A, while the voltage is regulated by the power supply itself, to deliver a certain power. The plasma power is measured using an oscilloscope (Tektronix TDS2012C), by integrating the product of voltage and current over a certain period of time. The voltage is measured using a high voltage probe (Testec) connected to the cathode. The current is obtained by measuring the voltage across a known resistance (3 Ω) that is placed in the grounding wire. The oscilloscope registers this as a voltage, which is converted to a current using Ohm's law.

Before each experiment the setup is flushed for 10 min with the gas mixture, after which the plasma is ignited, and another 10 min is given to stabilize. The exhaust gasses are stored in sample loops, each with a

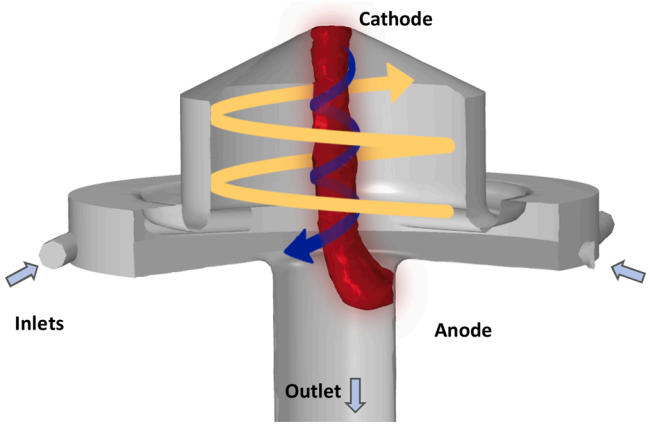

Fig. 1. Schematic picture of the GAP reactor, with illustration of the outer and inner vortex gas flows (yellow and blue arrows), and the plasma arc (red). The reactor body is at cathode potential while the outlet functions as anode. The arc is formed between the top of the cathode (top of the reactor body) and anode (outlet). The tangential gas inlets and the outlet of the reactor are indicated with arrows.

100 µl volume. After the filling process, the content of the sample loops is injected in the set of three columns with helium as carrier gas. For statistical analysis, every experiment is repeated three times, with four sample loops analyzed for each repeat, thus creating 12 data points. For every gas mixture a blank measurement without plasma is performed, needed to calculate the CO_2 and CH_4 conversion.

We measured the CO_2 and CH_4 conversion, as well as the H_2 and CO yield, the energy cost and energy efficiency of the conversion process. The formulas to calculate these properties are explained in detail in the Supporting information (Section S1).

3. Computational details

We used a modelling strategy based on four complementary models [31,32], which simulate the gas flow, the arc dynamics, the pathways of the gas molecules and the plasma chemistry in the reactor geometry of Fig. 1. These models are solved sequentially, in which each model builds further on the results of the previous model. We briefly describe here the four models in the sequence they are solved. The computational details of each of the models can be found in the Supporting information (Section S2).

3.1. Turbulent gas flow model

We describe the behaviour of the gas flow in the reactor by a turbulent gas flow model. Given the complex dual vortex flow in the reactor geometry and the high internal flow speed (up to 15 m/s at the inlet, for a flow rate of 10 l min^{-1}), a high level of turbulence is expected in the flow, which makes solving the classical Navier-Stokes equations in their full form computationally very intensive. For this reason, we simulate the gas flow using a Reynolds-averaged-Navier-Stokes (RANS) turbulent model, which significantly reduces the computation time by averaging all fluctuating turbulent quantities over time. The equations solved in this model are shown in the Supporting information (Section S2.1). These equations are decoupled from the plasma arc model in Section 3.2, so influences of the plasma on the flow behaviour are not taken into account. This decoupling was done to reduce the complexity of the 3D model and to limit calculation times. While this is an approximation, because in reality the high-temperature plasma will affect the flow behaviour, we believe that it is acceptable for this study, as we aim to reveal the effect of N_2 on the plasma process rather than to fully resolve the flow behaviour in our reactor geometry, which has already been done in previous studies[33]. The radial and axial flow velocity field, calculated by the turbulent gas flow model, are presented in the supporting information (Section S2.1). The computational domain in which the turbulent gas flow model is solved, is presented in Fig. 2. This domain consists of 1,016,694 mesh elements. The boundary conditions that apply for the inlet, outlet and wall boundaries are presented in the supporting information (Section S2.1). The physical properties of the CO_2-CH_4-N_2 mixture that are used as input for this model and for the models in the upcoming sections are also presented in the Supporting information (Section S2.2).

3.2. 3D plasma arc model

To simulate the gas breakdown and the arc formation and dynamics between the cathode and anode, we model the reactor geometry in Fig. 1 as part of an electric circuit. This circuit connects a 3 kV voltage source to the cathode, while keeping the walls grounded. The movement of the arc in the dual vortex gas flow is simulated by solving a current conservation equation based on Ohm's law. These equations as well as the electric circuit are shown in the Supporting information (Section S2.3). Additionally, this model calculates the rise in gas temperature and the corresponding rise in electric conductivity, as electric current flows through the gas between cathode and anode using the gas thermal balance equation, as shown in the Supporting information (also Section S2.3). As this heat transfer equation is coupled to the results of the turbulent flow model through the gas velocity field $\vec{u_g}$, the thermal plasma model can predict the position and movement of the arc within the double vortex gas flow. The calculated gas temperature, however, is overestimated in this model, as it assumes that the plasma is in thermal equilibrium, meaning that the gas temperature and electron temperature are equal at any point in the discharge. GA plasmas, however, are known to be "quasi-thermal" or "warm" plasmas, as the gas temperature is lower than the electron temperature. Indeed, the electrical energy is coupled to the electrons, and this rate of energy transfer from the electric field to the electrons is faster than the rate of energy transfer from the electrons to the heavy species, resulting in a thermal non-equilibrium between electrons and gas molecules. Our group already developed non-equilibrium models for gliding arc plasmas used for pure CO_2 conversion [33–35], but due to the complexity of the combined chemistry of the three input gasses CO_2-CH_4-N_2, resulting in 15987 reactions, we had to adopt here an equilibrium plasma model instead of a non-equilibrium model, because of its shorter calculation time (i.e. several hours instead of several days). This way the model can be solved for all gas feed ratios within a reasonable time. To compensate for the overestimation in the calculated gas temperature, we used the experimental energy efficiencies to correct how much power is actually lost to gas heating, by assuming

$$P_{heat} = P_{plasma}(100\% - EE) \quad (2)$$

In which P_{heat} is the power lost to gas heating, P_{plasma} is the experimental plasma power and *EE* is the experimental energy efficiency (see Supporting information Section S1, Eq. (16)). The heat source in the thermal balance equations is then normalized to deposit the corrected power P_{heat} to calculate the gas temperature, as shown by the equations in the Supporting information (also Section S2.3). The computational domain in which the plasma arc model is solved, is presented in Fig. 3. This domain consists of 505,116 mesh elements. The boundary conditions that apply for the inlet, outlet, anode and cathode boundaries are presented in the supporting information (Section S2.3). The approximations made in the turbulent flow and plasma arc model and their validity for this study are discussed in the Supporting information (Section S2.4).

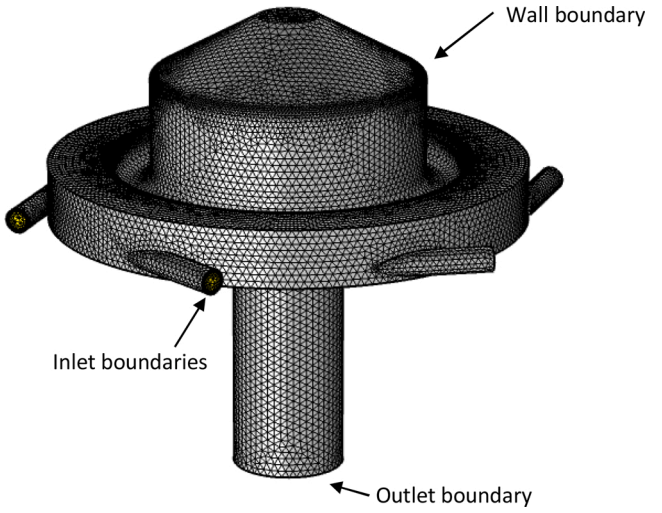

Fig. 2. Computational domain of the turbulent flow model. The inlets, outlet and wall boundaries are indicated.

3.3. Particle tracing simulations

Particle tracing simulations serve as the bridge between the previous 3D models and the following (chemical kinetics) model, by converting

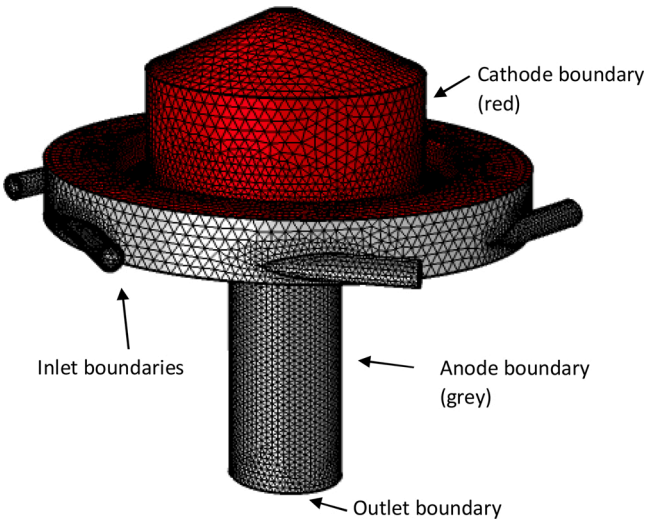

Fig. 3. Computational domain of the plasma arc model. The inlets, outlet, cathode and anode boundaries are indicated.

the calculated plasma parameters of the 3D models to a time-based input for the chemical kinetics model. The particle tracing simulations compute the trajectory of gas molecules through the reactor and report the gas temperature the molecules experience as a function of time, as they flow through the reactor. These trajectories are calculated based on the drag force imposed by the velocity fields that were previously computed by the 3D gas flow model.

$$\frac{d(m_p v)}{dt} = F \tag{3}$$

More information about the drag force can be found in the Supporting information (Section S2.5). We performed the trajectory calculations for 10,000 particles, i.e., gas molecules, to ensure statistically valid results. For each of these particles we assess if they flow through the plasma arc (where the power density is high and temperatures up to 3000 K are reached), or flow through the plasma afterglow in the reactor outlet (where the temperature still reaches up to a few 1000 K, but gradually cools down), or if they don't flow through the plasma at all. For each of these regimes, a chemical kinetics simulation is performed, calculating the underlying chemistry, the CH_4 and CO_2 conversion and product yields.

3.4. Quasi-1D chemical kinetics model

We use a quasi-one-dimensional (quasi-1D) chemical kinetics model to obtain better insight in the underlying chemistry of DRM in the GAP reactor. In principle, this is a 0D model, without spatial dimensions, and in which the plasma is modeled in a single point. Hence, the plasma properties (like species densities) only change as a function of time, allowing for the incorporation of an extensive plasma chemistry set, without suffering from long calculation times. In order to account for the spatial variations inside the GAP reactor, we use the particle tracing simulations to translate the output from the above 3D plasma model (i.e., the gas temperature as a function of position in the reactor) as input for this 0D model, i.e., temperature as a function of time. In this way, we obtain a quasi-1D model. We use the Zero-Dimensional Plasma Kinetics solver (ZDPlasKin) [36]. The mass conservation equation is solved for all the species included in the model, based on the production and loss terms, which are defined by the chemical reactions in the model. 177 species (various molecules, radicals, excited species and ions, as well as the electrons) are included, with 15987 reactions between them, i.e., various electron impact reactions, electron-ion recombination reactions, ion-ion, ion-neutral, and neutral-neutral reactions, as well as vibrational-translational (VT) and vibrational-vibrational (VV) relaxation reactions. Detail of the species and reactions involved, as well as the equations solved in the 0D model, are given in the Supporting information (Section S2.6).

4. Results and discussions

4.1. Absolute and effective CO_2 and CH_4 conversion

To analyse the effect of N_2 on the performance of DRM, we evaluated five different N_2 fractions (i.e. 0, 20, 40, 60 and 80 %), while the CO_2:CH_4 ratio was kept constant at 1:1. The total flow rate and electrical current were kept at 10 l min^{-1} and 0.3 A. To quantify the CO_2 and CH_4 conversion, we define both the absolute and the effective conversion. The absolute conversion, or simply "conversion", allows easy comparison between different mixtures, while the effective conversion takes into account the dilution of CO_2 and CH_4 in N_2. It is obtained by multiplying the absolute conversion with the CO_2 or CH_4 fraction in the mixture.

Fig. 4 presents the (absolute) CO_2 and CH_4 conversion as a function of N_2 fraction in the mixture, obtained in the experiments and the models. Without N_2, a conversion of 23.9 % is measured for CO_2 and 31.4 % for CH_4. These values rise notably upon N_2 addition, up to 47.7 % for CO_2 and 61.2 % for CH_4 at 80 % N_2. The calculated conversions are in satisfying agreement with the experimental values, except at 0 % N_2, where the calculated values are somewhat overestimated, and they drop towards 20 % N_2, while experimentally a rise in conversion is observed. This is attributed to the gas temperature, which may be somewhat overestimated in our model at 0 % N_2 and underestimated at 20 % N_2 (see later). Indeed, the gas temperature is self-consistently calculated in our plasma arc model, but this may be subject to some uncertainties. However, we prefer not to tune our calculations until perfect agreement is reached, without physical basis. We believe the agreement is reasonable, within the limitations and approximations of the models.

In general, our results demonstrate that the addition of N_2 benefits the conversion of CO_2 and CH_4. The reason is that N_2 does not actively participate in the DRM chemistry and essentially remains unconverted (i.e. less than 0.05 % conversion) in the plasma. As the energy acquired by N_2 molecules through inelastic collisions with electrons does not lead to chemical reactions, this energy eventually relaxes to gas heating, which accelerates the DRM reactions. This will be explained in more detail by the computational models in Section 4.5.

Note that by adding N_2, the total amount of CO_2 and CH_4 present in the gas mixture are lowered from 100 % (50 %-50 %) to 20 % (10 %-10 %). This means that the effective conversion of CO_2 and CH_4, which is calculated based on the initial fraction of each gas in the mixture (See the SI, Section S1) is expected to decrease upon adding more N2. The

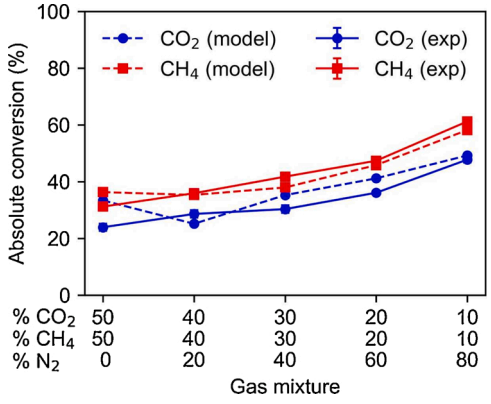

Fig. 4. Experimental and calculated absolute CO_2 and CH_4 conversion as a function of N_2 fraction.
The experiments in this figure were performed in triplicate, but the error bars on the experimental results are mostly too small to be visible.

effective CO_2, CH_4 and total (overall) conversion as a function of N_2 fraction are plotted in the SI (Fig. S5). The values drop from 12.0 to 4.8 % for CO_2, from 15.6 to 6.1 % for CH_4, and from 27.6 to 10.9 % for the total conversion, upon increasing N_2 fraction. Hence, while the absolute conversion increases upon N_2 addition, the effective and total conversion decreases, meaning that less CO_2 and CH_4 can be converted overall upon dilution, simply because there is less CO_2 and CH_4 present in the mixture. However, the drop in conversions is not linear: it is less steep at low N_2 fractions and becomes a bit more significant as more N_2 is added. This implies that at low N_2 fractions, the dilution effect is less important than the beneficial effect of N_2 on the (absolute) conversion, observed in Fig. 4.

4.2. Product yields

The measured and calculated product yields for different N_2 fractions are presented in Fig. 5(a). The CO yield rises from 26.1 to 42.1 %, while the H_2 yield rises from 25.2 to 49.8 %, upon increasing N_2 fraction. The calculated values are in satisfying agreement with the experiments. The model also predicts H_2O and C_2H_2 as important products, but they could not be measured by our GC. The CO and H_2 yields follow the same trend as the (absolute) conversion, which is logical. Fig. 5(b) illustrates the measured and calculated product selectivities. While the CO selectivity drops from 92.4 to 77.4 % upon increasing N_2 fraction, the H_2 selectivity first drops from 79.0 to 72.4 % when 20 % N_2 is added and then increases again to 81.2 % upon 80 % N_2 addition. Our model also predicts the drop in selectivity when 20 % N_2 is added, but the drops is much more pronounced and occurs for both CO and H_2. Our model suggests that for this mixing ratio, the selectivity towards C_2H_2 increases, which lowers the selectivity towards CO and H_2. As this drop is not so pronounced in the experiments, some reaction towards C_2H_2 may be slightly overestimated in the model at these low N_2 fractions, probably attributed to the somewhat underestimated gas temperature (see previous section).

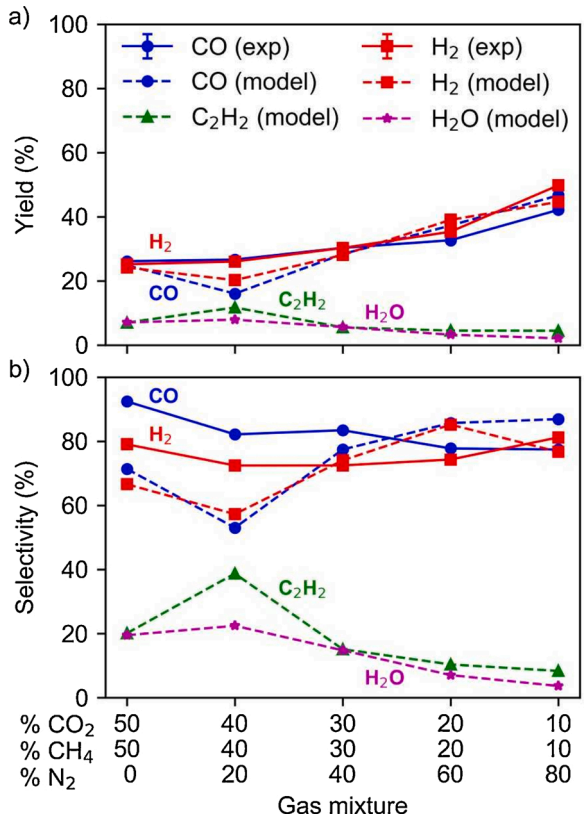

Fig. 5. Experimental and calculated product (a) yields and (b) selectivities, as a function of N_2 fraction. The experiments in both figures were performed in triplicate, but the error bars on the experimental results are too small to be visible.

4.3. Energy cost and energy efficiency

Besides conversion, product yields and selectivities, the other important criteria in defining the optimal gas composition for plasma-based DRM are the energy cost and energy efficiency, as they also define the performance of the process in an industrial context, where processes must be cost- and energy-efficient to be competitive. The energy efficiency is calculated from the effective conversion (shown in the SI; Fig. S5) and the specific energy input (SEI) of the process, the latter being defined by the ratio of the plasma power over the gas flow rate (see Supporting information Section S1, Eq. (12)). The experimental SEI across the different gas mixtures is presented in Fig. 6(a).

It is clear that the SEI significantly decreases when N_2 is initially added to the gas mixture, from 0.82 to 0.55 eV/molec (or from 3.2 to 2.2 kJ/L) when only 20 % N_2 is added to a pure CO_2-CH_4 mixture. Further addition of N_2 only induces a slight drop in SEI. The fact that less power is required to achieve a stable plasma at a fixed plasma current when N_2 is added, explains why N_2 is often added to pure CO_2, CH_4 or CO_2-CH_4 mixtures to achieve a more stable plasma discharge. While the origin of

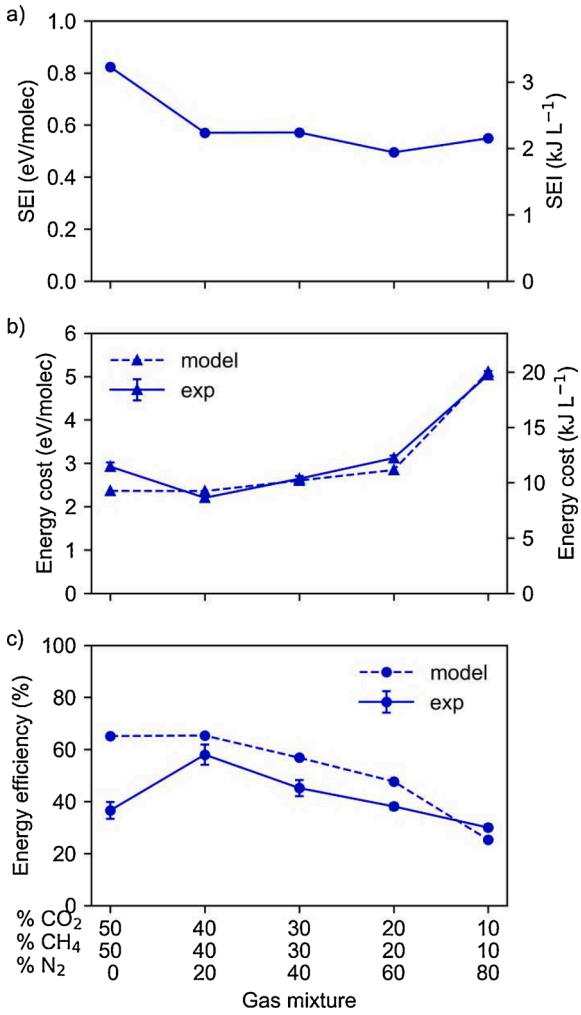

Fig. 6. a) Experimental SEI at a constant plasma current of 0.3 A, (b) experimental and calculated energy cost, and (c) experimental and calculated energy efficiency, as a function of N_2 fraction. For all three figures, the experiments were performed in triplicate, but the error bars on the experimental results are mostly too small to be visible.

this effect will be explained further by the computational models in Section 4.5, we will now discuss the implication of this effect on the energy cost and energy efficiency.

Fig. 6(b) depicts the energy cost (both in eV/molec and kJ/L) as a function of the N_2 fraction, obtained in the experiments and the models. Across the different gas mixtures, the energy cost ranges from 2.2 to 5.0 eV/molec (or 8.7 to 19.8 kJ/L) and has a minimum for an N_2 fraction of 20 %. The latter is attributed to the limited reduction in effective conversion at 20 % N_2 (i.e. only 2 % loss), as seen in the SI; Fig. S5), while it corresponds to a significantly lower SEI for stable plasma operation, as observed in Fig. 6(a), thus resulting in an overall lower energy cost. This minimum energy cost at the 20 % N_2 fraction corresponds to the maximum energy efficiency of 58 % as shown in Fig. 6(c), where the energy efficiency is plotted across the different gas mixtures, calculated using the formula in the Supporting information (Section S1 formula 16). The calculated energy cost and energy efficiency are in reasonable agreement with the measured values, except for the slope from 0 % to 20 % N_2. Indeed, the energy cost at 0% N_2 seems to be underestimated in the model (Fig. 6(b)), and the energy efficiency is somewhat overestimated (Fig. 6(c)). This is both explained by the overestimation in calculated CO_2 and CH_4 conversion at 0 % N_2, attributed to the gas temperature which is probably somewhat overestimated in our plasma arc model (see discussion in Section 4.1). In general, however, the agreement is reasonable, given the approximations in the models.

Taking it all together, our results indicate that 20 % N_2 addition yields the best performance, i.e., the lowest energy cost of 2.2 eV/molec (or 8.7 kJ/L) and highest energy efficiency of 58 %, for a CO_2 and CH_4 (absolute) conversion of 28.7 and 35.9 %, and a total conversion of 25.8 %.

4.4. Comparison with other plasma reactors

Table 1 compares our best results with recent DRM results of different types of gliding arc (GA) plasmas reported in literature. Our GAP reactor achieves a relatively low energy cost, but is outmatched by some other GA reactors in terms of conversion. Results obtained with the same type of GAP reactor for a pure CO_2-CH_4 mixture by Cleiren et al. [16] show a slightly higher energy cost of 2.5 eV/molec (or 10 kJ/L) with significantly lower conversion of 18 and 10 % for CO_2 and CH_4, respectively. In that study, however, a less optimal CH_4/CO_2 ratio of 75/25 (instead of 50/50) was used, which was needed to sustain a stable plasma in the absence of N_2. Results obtained for a "rotating gliding arc" (RGA) reactor by Martin-del-Campo et al. [19] show a much lower conversion of 12.8 and 10.9 % for CO_2 and CH_4, respectively, with a higher energy cost of 14.4 eV/molec (or 56.5 kJ/L). Also the "rotating gliding arc discharge" (RGAD) reactor of Lu et al. [20] achieves lower conversion with a higher energy cost of 5.9 eV/molec (or 23.3 kJ/L). More competitive results were shown for another RGA reactor by Wu et al. [12], achieving a higher conversion of 35 and 36 % for CO_2 and CH_4, respectively, at a very low energy cost of 1 eV/molec (or 3.9 kJ/L). As mentioned in the introduction, to our knowledge this is the lowest energy cost for a gliding arc reactor reported up to now in literature. However, it should be noted that this reactor uses a magnetic field to enhance the plasma and improve the performance, which is a more complex setup and thus less viable for industrial applications. Significantly higher conversion of 52.3 and 58.9 % for CO_2 and CH_4, respectively, were achieved by the "alternating current gliding arc" (AC-GA) reactor of Xia et al., [17] but at a higher energy cost of 6.5 eV/molec (or 25.5 kJ/L). The highest conversions are obtained by the "arc plasma reactor" (APR) of Dinh et al. [18], reaching up to 49 and 74 % for CO_2 and CH_4 respectively, which is almost twice the values obtained in our work. However, the energy cost is also more than double compared to our value, reaching 4.6 eV/molec (or 18.1 kJ/L). In this study a fraction of 50 % N_2 was used to stabilise the plasma arc. When interpolating our results between 40 % and 60 % N_2 fraction and comparing them with the data of the APR, we obtain conversions of 33.2 and 44.6 % for CO_2 and CH_4, respectively, which are still a bit lower than in the APR, especially for CH_4, but our energy cost of 2.9 eV/molec (or 11.4 kJ/L) in this case is also still significantly lower. It should also be noted that the use of a correction factor for gas expansion, which is crucial to obtain the correct conversion as explained in the supporting information (Section S1), could only be confirmed for the GAP and APR reactors, so the other results from literature should be interpreted carefully as the conversion might be overestimated.

In Fig. 7, we benchmark our results to an extended range of DRM data of several different plasma reactor types collected by Snoeckx and Bogaerts [3]. Our data points are added to this figure as orange stars. Except for the mixture with the highest N_2 fraction, they are all located above the energy cost target of 4.27 eV/molecule (cf. green dash-dotted line indicated as "efficiency target"), which was calculated by Snoeckx and Bogaerts [3] as the target energy cost to be competitive in terms of syngas production with other technologies. Note that the y-axis is reversed, from the highest to the lowest energy costs (i.e., the best values are at the top). Our results perform well in terms of energy cost, i.e., better that DBD, MW and corona discharges, which can achieve high conversions up to 90 %, but always at an energy cost above 10 eV/molecule. Nevertheless, our results do not yet reach the best data obtained by some APGD and other GA discharges, but we believe there is room for future improvements of our GAP reactor. Indeed, increasing

Table 1
Key performance indicators for DRM, comparing our best results with different types of gliding arc plasmas from literature.

Reactor type	Gas mixture	CO_2 conversion (%)	CH_4 conversion (%)	EC (eV/molec) (EC (kJ/L))	Ref.
GAP	40 % CO_2, 40 % CH_4, 20 % N_2	28.6	35.6	2.2 (8.6)	This work
GAP	75 % CO_2, 25 % CH_4	18	10	2.5 (10)	[16]
RGA	50 % CO_2, 50 % CH_4	12.8	10.9	14.4 (56.5) [a]	[19]
RGAD	60 % CO_2, 40 % CH_4	17.0	28.1	5.9 (23.3) [a]	[20]
RGA	50 % CO_2, 50 % CH_4	36	35	1.53 (6.0) [a]	[12]
AC-GA	60 % CO_2, 40 % CH_4	52.3	58.9	6.5 (25.5) [a]	[17]
APR	37.5 % CO_2, 12.5 % CH_4, 50 % N_2	49	74	4.6 (18.1) [a]	[18]

[a] value not provided in the reference but calculated using the provided data.

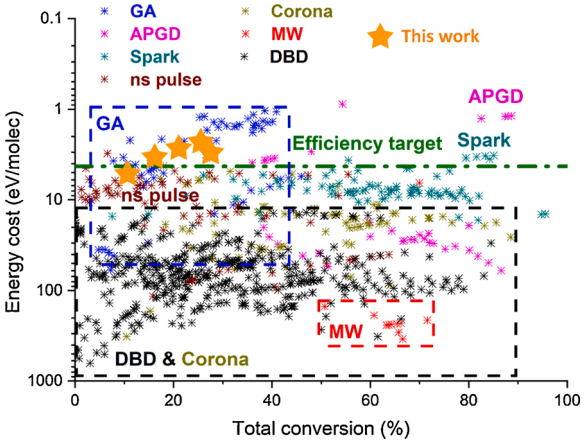

Fig. 7. Comparison of energy cost as a function of total conversion for DRM, in various types of plasma reactors from literature. Original figure obtained from Snoeckx and Bogaerts [3]. Our results are added to the graph as orange stars.

the fraction of gas that is treated by the plasma arc, through changes in the reactor design, would significantly increase the conversion, and hence also the energy efficiency of the GAP. This will be studied in our future work. Nevertheless, the fact that our results show an energy cost already better than the efficiency target defined by Snoeckx and Bogaerts [3] indicates the potential of our GAP reactor for DRM with industrial gas emissions containing N_2.

4.5. Explanation of the performance by means of the computational models

As the calculated conversions, product yields and selectivies, and the energy cost and energy efficiency are all in satisfying agreement with the experiments, we can use our models to explain the experimental trends upon addition of N_2 to the CO_2-CH_4 mixture. The physical properties of the plasma are captured by the 3D models, while the chemical reaction pathways are calculated by the quasi-1D model.

4.5.1. N_2 addition enhances the plasma arc temperature

To calculate the physical properties of the plasma, the arc formation and stabilization in the vortex gas flow of the GAP are simulated in 3D by the arc plasma model. The arc is initially formed at the shortest distance between cathode and anode and is dragged to the centre of the reactor by the rotational vortex flow [37]. The result of this stabilization is depicted in Fig. 8, showing the arc position (in red) within the velocity streamlines, as calculated by our turbulent gas flow model and plasma arc model. As shown in the figure, the gas enters the reactor through the inlets at high gas velocities (10−14 m/s) and rotates upwards along the reactor wall at a high gas velocity. At the top of the reactor, the vortex reverses and the gas flows downwards through the center of the reactor, slowing down to a lower gas velocity (4−6 m/s). The radial and axial flow velocity field, calculated by the turbulent gas flow model, are presented in the supporting information (Section S2.1). The arc is indeed stabilized by the vortex flow in the middle of the reactor, gliding over the anode outlet wall, while it remains connected to the top of the cathode. Our model predicts that 38 % of the gas gets treated directly by the plasma, either by the steady part of the arc (15 %) or by the rotating part of the arc (23 %), which glides along the outlet wall, while up to 11.8 % of the gas is treated by the hot afterglow of the plasma. More details about the gas fractions that flow through the arc and afterglow are given in the Supporting information (Section S2.6, table S5). It also means that at least 50 % of the gas is not yet treated by the plasma (or hot afterglow), showing the clear room for further improvement in conversion, by smart reactor design, as mentioned in previous section.

The calculated arc dimensions in Fig. 8 very strongly resemble the arc dimensions calculated by Trenchev et al. [33] in a two-dimensional non-thermal plasma model for pure CO_2 in the GAP, which indicates that our approach of the 3D thermal plasma (with corrected gas temperature) correctly predicts the shape of the arc. Further benchmarking of our approach to the non-thermal plasma model of Trenchev et al. can be found in the supporting information (Section S4).

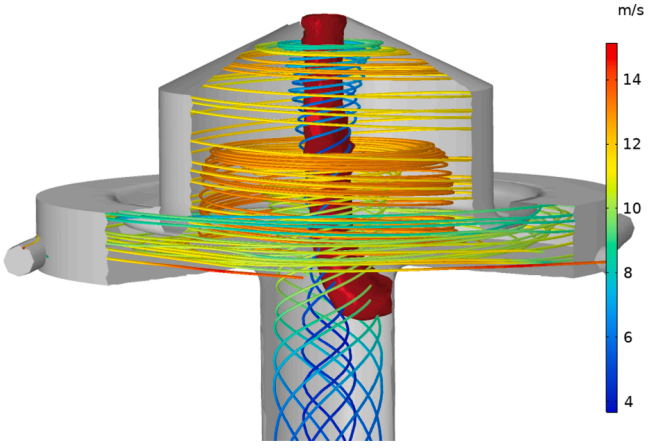

Fig. 8. Calculated gas velocity streamlines (see colour scale at the right) and arc formation in the GAP reactor for a 10 l/min 50/50 CO_2/CH_4 flow. The results look the same for all gas mixtures investigated.

Fig. 9 illustrates the 2D gas temperature profile, calculated by the thermal plasma model for a pure CO_2-CH_4 mixture and corrected using the experimental plasma power and energy efficiency (see Section 3.2 above). Inside the arc the gas temperature builds up to 3200 K in the centre of the arc. This value is very close to the temperature calculated for a pure CO_2 plasma in the GAP by Trenchev et al. [33] which indicates that our approach of using the experimental energy efficiency to determine how much power is put into gas heating, delivers realistic temperature values. Further benchmarking of our approach to the non-thermal plasma model of Trenchev et al. can be found in the supporting information (Section S4). Note that the gas temperature plays a crucial in DRM, since the production rate of reactive plasma species, and thus also the overall rate of the conversion process, increases significantly upon higher gas temperatures.

Our models reveal that the gas temperature is heavily influenced by the composition of the gas mixture. This is illustrated in Fig. 10 for the maximum gas temperatures achieved in the arc across the different gas mixtures, as calculated by the arc plasma model. In general, the temperature in the arc increases upon N_2 addition, reaching up to 4400 K for a N_2 fraction of 80 %. Firstly, this is attributed to the higher overall heat capacity upon N_2 addition, as illustrated by the isobaric heat capacity of the different CO_2-CH_4-N_2 mixtures at 3000 K (i.e. a typical plasma gas temperature) in Fig. 10 (right y-axis). Indeed, the addition of N_2 lowers the overall heat capacity of the mixture, meaning that less energy is required to heat the gas mixture at higher N_2 fractions. The reason is that a diatomic molecule (like N_2) has less internal degrees of freedom (rotational, vibrational) than polyatomic molecules (like CO_2 and CH_4) and thus stores more of its energy in its translational degrees of freedom, making it easier to heat up the gas when N_2 is present in the mixture, for the same input (plasma) power.

Next to the lower heat capacity of the mixture, the more efficient gas heating upon N_2 addition is also because N_2 channels more of the applied (plasma) energy into gas heating. While some N_2 molecules acquire enough energy through inelastic collisions with electrons to be ionized or to dissociate, most molecules do not undergo chemical reactions because of the strong triple bond, and only become (vibrationally) excited, after which they eventually relax their acquired energy, increasing the gas temperature in the plasma. Note that in Fig. 10 the gas temperature for the pure CO_2-CH_4 mixture is higher than when 20 % N_2 is added, which does not align with the trend observed in the other gas mixtures. This is due to the fact that at the fixed plasma current of 0.3 A, this gas mixture operates at a significantly higher SEI (see Fig. 6 (a))

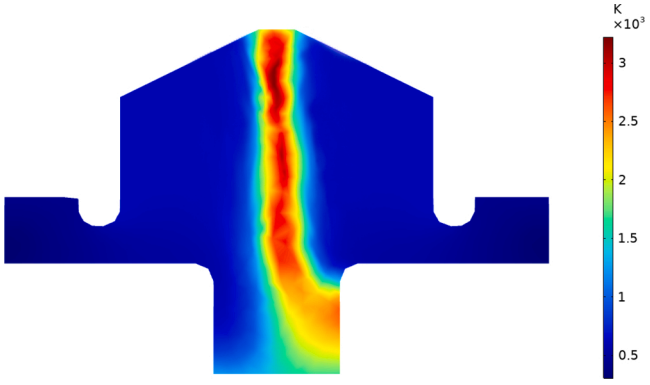

Fig. 9. Calculated 2D gas temperature profile in the GAP for a pure (50/50) CO_2-CH_4 plasma, at 10 l/min and 0.3 A electric current.

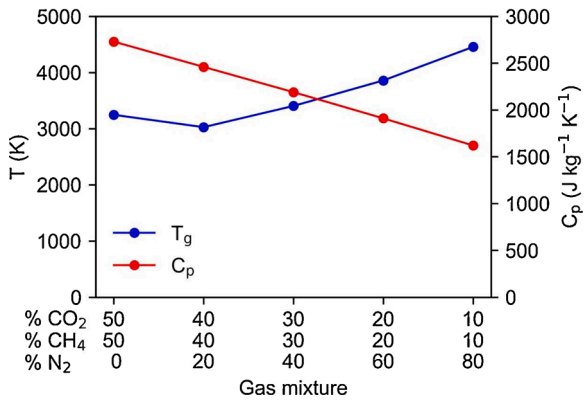

Fig. 10. Maximum calculated gas temperature in the plasma (arc centre) (blue) and isobaric heat capacity of the CO_2-CH_4-N_2 gas mixture at 3000 K (red), as a function of the N_2 fraction.

compared to the other mixtures, so that more power is available to put in to gas heating, which outweighs the effect of the N_2 addition.

The higher gas temperature resulting from N_2 addition has also been observed experimentally in a CH_4 plasma by Zhang et al. for a rotating gliding arc reactor [38]. Using optical emission spectroscopy the authors observed an increase of more than 300 K when the molar CH_4/N_2 ratio was reduced from 1.20 to 0.05. A similar observation has been reported by Gröger et al. when studying a pure N_2 plasma in the GAP reactor using optical emission spectroscopy [39]. Gas temperatures up to 5500 K were measured, which is much higher that the gas temperatures between 3000 and 4000 K calculated by Trenchev et al. for a pure CO_2 plasma in the same GAP reactor [33].

The higher gas temperature speeds up the plasma kinetics of the DRM reactions, and this explains the higher (absolute) CO_2 and CH_4 conversions at higher N_2 fractions (see Fig. 4). These results provide valuable new insights in addition to previous computational studies that analysed the beneficial effect of N_2 addition to CO_2 or CO_2/CH_4 plasmas in various plasma reactor types [22–25]. In a dielectric barrier discharge (DBD) reactor, modelling revealed that N_2 improved the CO_2 conversion through reaction with metastable electronically excited $N_2(\Sigma_u^+)$ molecules [22], while in a microwave (MW) plasma reactor at reduced pressure, N_2 enhanced the CO_2 conversion by transferring its vibrational energy to CO_2 molecules through vibration-vibrational relaxation reactions [24]. The DBD and MW plasma operate at lower gas temperatures than our GAP (300 K for the DBD and 1000 K for the MW plasma at reduced pressure) and, as a consequence, thermal conversion of CO_2 or CH_4 is not so prominent, unlike in our GAP reactor (see below). Our study thus perfectly complements previous modeling results, providing new insights for warm plasmas, where thermal conversion and the effects of the gas temperature are crucial.

4.5.2. N_2 addition enhances the electron density, affecting the plasma conductivity, plasma power and SEI

As illustrated in Fig. 6(a) above, the measured SEI in the CO_2-CH_4 mixture drops significantly when 20 % N_2 is added, due to the lower power needed to ignite and sustain the plasma at a fixed plasma current. Our computational models reveal that this is attributed to the increasing electron density upon adding N_2 to the mixture, as illustrated in Fig. 11 (black line, left y-axis). This figure also presents the dominant electron formation reactions in the mixture (coloured bars, right y-axis), as calculated by the quasi-1D model. Note that this model was run for a constant temperature of 3500 K and power density of 4.5 kW cm^{-3}, to clearly isolate the effect of the changing gas composition (independent from the effect of the gas temperature) on the plasma chemistry. Without N_2, electron formation mainly occurs through recombination of H_2 and O- to H_2O (reaction 5), and of CO and O- to CO_2 (4), as well as by electron impact ionization of CO_2 (reaction 1). When N_2 is added, ionization of N_2 (especially electron impact ionization of ground state N_2 (reactions 7 and 8), but also associative ionization by two electronically excited molecules, $N_2(A^1\Sigma_u)$ (reaction 9) and $N_2(A^3\Sigma_u)$) (reaction 10) take over as the main electron formation processes, explaining the rising electron density in the plasma. In other words, through the addition of N_2 a new gas is introduced to the plasma, which, unlike CO_2 and CH_4, does not react away easily by other (chemical) reactions due to its strong triple bond, and is thus always available for ionization. The electron density enhances the conductivity of the plasma, thus reducing the power needed to achieve a certain plasma current. Hence, this explains the drop in plasma power, and thus in SEI (cf. Fig. 6(a)) upon N_2 addition, contributing to the low energy cost of the 20 % N_2 mixture.

4.5.3. Underlying reaction pathways in DRM

A general reaction scheme, as predicted by our quasi-1D simulations, is presented in Fig. 12, indicating the important reactions involved in the conversion processes of CO_2 and CH_4 and their link to the formation processes of the most abundant products, i.e., CO, H_2, H_2O and C_2H_2.

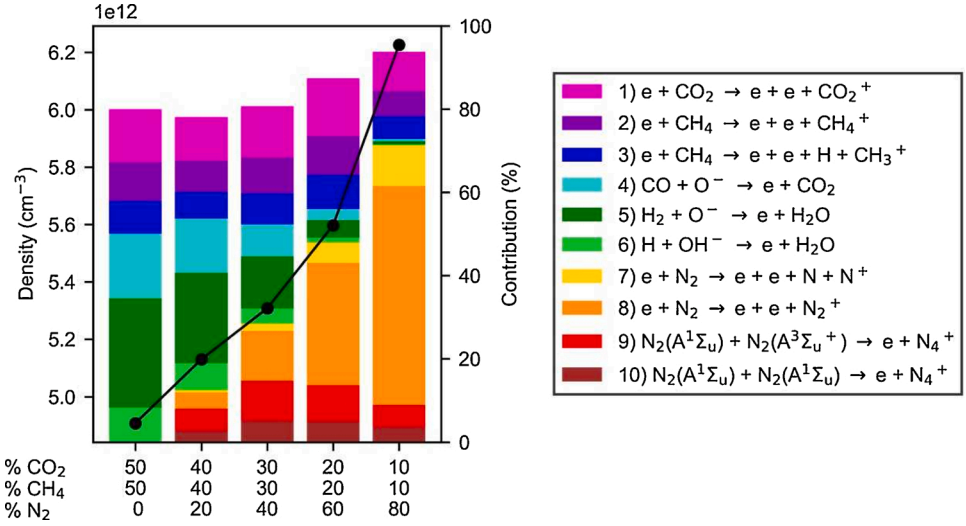

Fig. 11. Calculated electron density (black line, left y-axis) as a function of N_2 fraction, at a constant gas temperature of 3500 K and power density of 4.5 kW cm^{-3}. The coloured bars (right y-axis) show the contribution of the dominant electron formation reactions across the different gas mixtures. The values are determined for a plasma residence time of 1 ms, which is comparable to the residence time in the plasma obtained in the 3D simulations based on the experimental conditions.

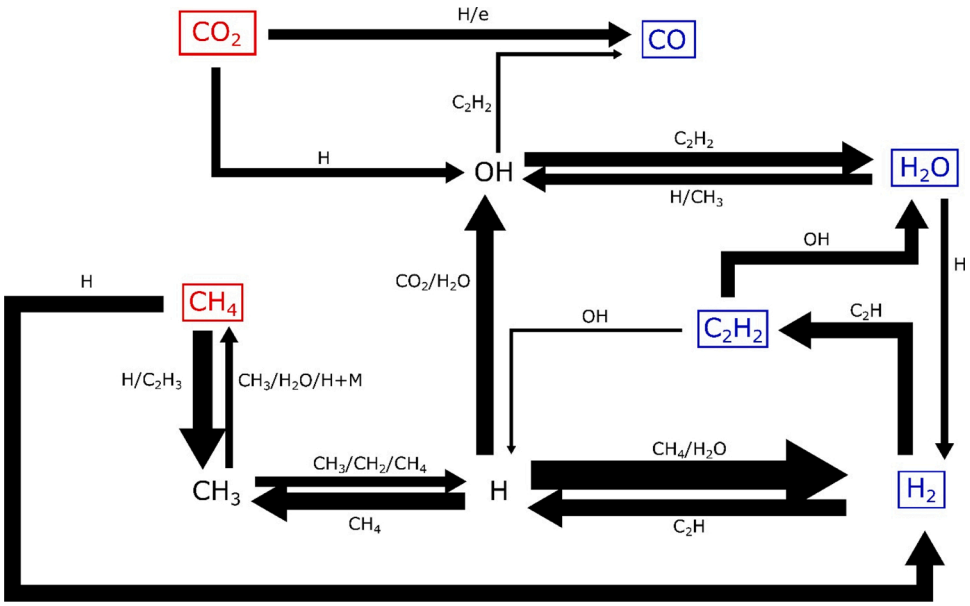

Fig. 12. Schematic overview of the most important reactions for the conversion of CO_2 and CH_4 and the formation of CO, H_2, C_2H_2 and H_2O, based on the time-averaged net reaction rates for the CO_2-CH_4-N_2 gas mixture with 40 % N_2. The arrow thickness is indicative of the net reaction rate of the reactions involved. The arrows towards CO are clearly thinner than towards H_2, while nearly equal amounts of CO and H_2 are formed. The reason is that loss processes for CO are less important than for H_2 (see scheme). Note that N_2 does not play a direct role in this chemistry, except as neutral molecule (M), but it has an important indirect contribution, through the enhanced gas temperature and electron density (see before).

The figure applies to the CO_2:CH_4:N_2 mixture with 40 % N_2, which is intermediate, and thus representative for the various N_2 fractions. The thickness of the arrows is indicative of the total time-averaged rate (averaged over the residence time in the plasma) and thus marks the importance of the reaction within the DRM process. Note that these are all net rates, balancing the rates of the forward and reverse reactions. The reactants of the dominant reactions are placed next to the arrows.

The scheme in Fig. 12 shows that CH_4 conversion is mostly driven by reactions with H and C_2H_3 to form CH_3 (Eqs. (4) and (5)) and H_2 (Eq. (4)). CH_4 is also converted upon reactions with O or electrons, but because of their lower contribution (< 3 %), these reactions are not displayed in the scheme. The relative importance of electron impact reactions decreases with increasing N_2 fraction, in spite of the higher electron density, because the contribution of the heavy species reactions increases strongly at the high gas temperatures characteristic for the high N_2 fractions (cf. Fig. 10). Higher N_2 fractions thus promote the thermal DRM chemistry, rather than electron-induced reactions.

$$CH_4 + H \rightarrow CH_3 + H_2 \quad (4)$$

$$H_4 + C_2H_3 \rightarrow CH_3 + C_2H_4 \quad (5)$$

CH_3 can react back to CH_4 through three-body recombination with H and M (representing any neutral molecule) (Eq. (6)) or upon reactions with CH_3 or H_2O (Eqs. (7) and (8)). In addition, it can react further with CH_3, CH_2 and CH_4, creating H atoms and multiple C_2H_x species (Eqs. (9) and (11)). The formation to H_2 occurs upon reaction of H atoms with CH_4 (Eq. (4)) or with H_2O (Eq. (12)). Recombination of 2 H atoms into H_2 occurs as well, but at a much lower rate.

$$CH_3 + H + M \rightarrow CH_4 + M \quad (6)$$

$$CH_3 + CH_3 \rightarrow CH_4 + CH_2 \quad (7)$$

$$CH_3 + H_2O \rightarrow CH_4 + OH \quad (8)$$

$$CH_3 + CH_3 \rightarrow H + C_2H_5 \quad (9)$$

$$CH_3 + CH_2 \rightarrow H + C_2H_4 \quad (10)$$

$$CH_3 + CH_4 \rightarrow H + C_2H_6 \quad (11)$$

$$H + H_2O \rightarrow H_2 + OH \quad (12)$$

The main conversion pathway for CO_2 proceeds through reactions with H and (to a smaller extent) electrons (Eqs. (13) and (14)), creating CO and OH (or O). Like for CH_4, the relative contribution of electron impact dissociation of CO_2 decreases upon higher N_2 fractions, as the higher gas temperature promotes the thermal reactions between the heavy species. While dissociation from CO_2 is the most important formation reaction for CO, another (less important) CO formation pathway is by reaction of OH and C_2H_2 (Eq. (15)). Several loss reactions of CO exist towards CO_2, O and CH_3, but they are not added to the scheme, because their rates are several orders of magnitudes lower than the formation pathways.

$$CO_2 + H \rightarrow CO + OH \quad (13)$$

$$CO_2 + e \rightarrow CO + O + e \quad (14)$$

$$OH + C_2H_2 \rightarrow CO + CH_3 \quad (15)$$

C_2H_2 is mainly formed upon reaction of H_2 with C_2H (Eq. (16)), which is also the major loss reaction for H_2. C_2H_2 has two different loss reactions with OH, i.e., a small fraction forms H (Eq. (17)) while the majority is lost towards H_2O (Eq. (18)). The latter reaction is also the major loss process of OH. Finally, H_2O is converted again to H_2 upon reaction with H (Eq. (12)), and to OH upon reactions with CH_3 or H (Eqs. (8) and (12)).

$$H_2 + C_2H \rightarrow H + C_2H_2 \quad (16)$$

$$C_2H_2 + OH \rightarrow H + CH_2CO \quad (17)$$

$$C_2H_2 + OH \rightarrow H_2O + C_2H \quad (18)$$

5. Conclusions

In this paper, we investigated the effect of N_2 on plasma-based DRM in a gliding arc plasmatron, by means of experiments and a combination of four different computational models. Overall, a N_2 content of 20 % was found to be optimal in terms of overall performance, achieving a total conversion of 25.8 %, and (absolute) conversions of 28.6 % for CO_2 and 35.9 % for CH_4 at a total energy cost of 2.2 eV/molec (or 8.7 kJ/L) and energy efficiency of 58 %. The syngas components (CO and H_2) are the major products, but the model reveals that some C_2H_2 (and H_2O) are also formed. Our results are among the best reported in literature for plasma-based DRM, when comparing with many other plasma types, certainly considering the low energy cost and high energy efficiency

achieved. For the conversion, we still see room for improvement, by increasing the fraction of gas that flows through the plasma arc, by smart reactor design optimisation.

Our computational models yield good agreement with the experimental conversions, product yields and selectivities, energy cost and energy efficiency, and can thus be used to elucidate the underlying mechanisms, and explain the trends of N_2 addition. The models reveal that the addition of N_2 significantly increases the gas temperature in the plasma. This is attributed to the lower isobaric heat capacity, and because N_2 remains largely unconverted in the plasma, so virtually all plasma energy that is taken up by N_2 molecules through inelastic collisions with electrons is eventually distributed to the translational degrees of freedom. Hence, the maximum gas temperature reached in the plasma significantly increases, from around 3200 K without N_2, up to 4400 K upon 80 % N_2 addition. This higher temperature accelerates the DRM reactions, enhancing the (absolute) conversions of CO_2 and CH_4.

Indeed, our models reveal that the addition of N_2 promotes the conversion of CO_2 and CH_4 through thermal conversion reactions, rather than through electron impact reactions. Due to the higher gas temperature at higher N_2 fractions, the rates of the thermal chemistry reactions increase significantly, so these reaction pathways have the highest contribution in the conversion process.

Next to increasing the gas temperature, the addition of N_2 also reduces the power that is needed to achieve a certain plasma current, and thus the plasma can operate at lower SEI, for a constant gas flow rate. Indeed, the N_2 molecules are virtually not dissociated (and thus converted in chemical reactions), but they only undergo ionization (and excitation). This enhances the electron production rate due to the extra ionization channels, thus increasing the electron density. A higher electron density leads to a higher plasma conductivity, so less power is required to achieve the plasma current of 0.3 A when more N_2 is present, thereby reducing the SEI of the process.

Hence, both the higher absolute conversion and lower SEI at increasing N_2 fractions are beneficial, but on the other hand, diluting the CO_2-CH_4 fraction reduces the effective conversion of CO_2 and CH_4. However, at N_2 fractions around 20 %, the advantages of adding N_2 outweigh the dilution effect, improving the energy efficiency of the process with respect to pure CO_2-CH_4 mixtures, by 21 %, i.e., from 37 to 58 %, and reducing the energy cost from 2.9 to 2.2 eV/molec (or from 11.5 to 8.7 kJ/L). While these values are reported specifically for our GAP reactor at the operating conditions mentioned (i.e. flow rate of 10 l/min and current of 0.3 A), these trends are expected to be valid for a wider range of conditions. According to our model predictions, the benefits of adding N2 (i.e. (i) reducing the SEI and (ii) increasing the gas temperature) are not related to the gas flow rate, plasma current or reactor geometry, and are thus expected to occur in other quasi-thermal plasma reactors as well.

In conclusion, we have shown that the addition of N_2, a ubiquitous component in many industrial emissions, can significantly improve the energy efficiency of plasma-based DRM, thus bringing this plasma-based process a step closer towards real applications.

Author statement

Senne Van Alphen: Methodology, Investigation, Writing- Original draft preparation, Writing- Reviewing and Editing

Joachim Slaets: Investigation, Writing- Original draft preparation, Visualization

Sara Ceulemans: Investigation

Maryam Aghaei: Methodology, Investigation, Project administration

Rony Snyders: Supervision, Funding acquisition, Writing- Reviewing and Editing

Annemie Bogaerts: Supervision, Funding acquisition, Writing- Reviewing and Editing, Project administration

Declaration of Competing Interest

The authors declare that they have no known competing financial interests or personal relationships that could have appeared to influence the work reported in this paper.

Acknowledgements

This research was supported by the European Research Council (ERC) under the European Union's Horizon 2020 research and innovation programme (grant agreement No 810182 – SCOPE ERC Synergy project), the Excellence of Science FWO-FNRS project (FWO grant ID GoF9618n, EOS ID 30505023), and through long-term structural funding (Methusalem). The calculations were performed using the Turing HPC infrastructure at the CalcUA core facility of the Universiteit Antwerpen (UAntwerpen), a division of the Flemish Supercomputer Center VSC, funded by the Hercules Foundation, the Flemish Government (department EWI) and the UAntwerpen.

Appendix A. Supplementary data

Supplementary material related to this article can be found, in the online version, at doi:https://doi.org/10.1016/j.jcou.2021.101767.

References

[1] R.K. Pachauri, L.A. Meyer, Climate Change 2014: Synthesis Report. Contribution of Working Groups I, II and III to the Fifth Assessment Report of the Intergovernmental Panel on Climate Change, Geneva, Switzerland, 2014, 2014.
[2] W. McDonough, M. Braungart, P.T. Anastas, J.B. Zimmerman, Applying the principles of green engineering to cradleto-cradle design, Environ. Sci. Technol. 37 (2003) 434A–441A.
[3] R. Snoeckx, A. Bogaerts, Plasma technology – a novel solution for CO_2 conversion? Chem. Soc. Rev. 46 (2017) 5805–5863.
[4] V. Kumaravel, J. Bartlett, S.C. Pillai, Photoelectrochemical conversion of carbon dioxide (CO2) into fuels and value-added products, ACS Energy Lett. 5 (2020).
[5] B. Hu, C. Guild, S.L. Suib, Thermal, electrochemical, and photochemical conversion of CO2 to fuels and value-added products, J. CO2 Util. 1 (2013) 18–27.
[6] G. Centi, S. Perathoner, Turning CO2 into valuable chemicals, Catal. Today 148 (2009) 191–205.
[7] F.A. Rahman, M.M.A. Aziz, R. Saidur, W.A.W.A. Bakar, M. Hainin, R. Putrajaya, N. A. Hassan, Pollution to solution: capture and sequestration of carbon dioxide (CO2) and its utilization as a renewable energy source for a sustainable future, Renew. Sustain. Energy Rev. 71 (2017) 112–126.
[8] A. Bogaerts, E.C. Neyts, Plasma technology: an emerging technology for energy storage, ACS Energy Lett. 3 (2018) 1013–1027.
[9] A. Fridman, Plasma Chemistry, Cambridge University Press, Cambridge, U.K, 2008.
[10] L. Wang, Y. Yi, C. Wu, H. Guo, X. Tu, One-step reforming of CO2 and CH4 into high-value liquid chemicals and fuels at room temperature by plasma-driven catalysis, Angew. Chem. 129 (2017) 1367–13871.
[11] M. Scapinello, L.M. Martini, T. Tosi, CO2 hydrogenation by CH4 in a dielectric barrier discharge: catalytic effect of Ni and Cu, Plasma Process. Polym. 11 (2014) 624–628.
[12] A. Wu, J. Yan, H. Zhang, M. Zhang, C. Du, X. Li, Study of the dry methane reforming process using a rotating gliding arc reactor, Int. J. Hydrogen Energy 39 (2014) 17656–17670.
[13] M. Scapinello, L.M. Martini, G. Dilecce, P. Tosi, Conversion of CH4/CO2 by a nanosecond repetitively pulsed discharge, J. Phys. D Appl. Phys. 49 (2016), 075602.
[14] W.C. Chung, M.B. Chang, Review of catalysis and plasma performance on dry reforming of CH4 and possible synergistic effects, Renew. Sustain. Energy Rev. 62 (2016) 13–31.
[15] D. Li, X. Li, M. Bai, X. Tao, S. Shang, X. Dai, Y. Yin, CO2 reforming of CH4 by atmospheric pressure glow discharge plasma: a high conversion ability, Int. J. Hydrogen Energy 34 (2009) 308–313.
[16] E. Cleiren, S. Heijkers, M. Ramakers, A. Bogaerts, Dry reforming of methane in a gliding arc plasmatron: towards a better understanding of the plasma chemistry, ChemSusChem 10 (2017) 3864.
[17] Y. Xia, N. Lu, B. Wang, J. Li, K. Shang, N. Jiang, Y. Wu, Dry reforming of CO2–CH4 assisted by high-frequency AC gliding Arc discharge: electrical characteristics and the effects of different parameters, Int. J. Hydrogen Energy 42 (2017) 22776–22785.
[18] D.K. Dinh, G. Trenchev, D.H. Lee, A. Bogaerts, Arc plasma reactor modification for enhancing performance of dry reforming of methane, J. CO2 Util. 42 (2020), 101352.
[19] J. Martin-del-Campo, S. Coulombe, J. Kopyscinski, Influence of operating parameters on plasma-assisted dry reforming of methane in a rotating gliding arc reactor, Plasma Chem. Plasma Process. 40 (2020) 857–881.

[20] N. Lu, D. Sun, Y. Xia, K. Shang, B. Wang, N. Jiang, J. Li, Y. Wu, Dry reforming of CH4–CO2 in AC rotating gliding Arc discharge: effect of electrode structure and gas parameters, Int. J. Hydrogen Energy 43 (2018) 13098–13109.
[21] J. Slaets, M. Aghaei, S. Ceulemans, S. Van Alphen, A. Bogaerts, CO2 and CH4 conversion in "real" gas mixtures in a gliding Arc plasmatron: how do N2 and O2 affect the performance? Green Chem. 22 (2020) 1366–1377.
[22] R. Snoeckx, S. Heijkers, K. Van Wesenbeeck, S. Lenaerts, A. Bogaerts, CO2 conversion in a dielectric barrier discharge plasma: N2 in the mix as a helping hand or problematic impurity? Energy Environ. Sci. 9 (2016) 999–1011.
[23] W. Wang, R. Snoeckx, X. Zhang, M.S. Cha, A. Bogaerts, Modeling plasma-based CO2 and CH4 conversion in mixtures with N2, O2, and H2O: the bigger plasma chemistry picture, J. Phys. Chem. C 122 (2018) 8704–8723.
[24] S. Heijkers, R. Snoeckx, T. Kozák, T. Silva, T. Godfroid, N. Britun, R. Snyders, A. Bogaerts, CO_2 conversion in a microwave plasma reactor in the presence of N_2: elucidating the role of vibrational levels, J. Phys. Chem. C 119 (2015) 12815–12828.
[25] M. Ramakers, S. Heijkers, T. Tytgat, S. Lenaerts, A. Bogaerts, Combining CO2 conversion and N2 fixation in a gliding arc plasmatron, J Co2 Util. 33 (2019) 121.
[26] R. Snoeckx, K. Van Wesenbeeck, S. Lenaerts, M.S. Cha, A. Bogaerts, Suppressing the formation of NO: X and N2O in CO2/N2 dielectric barrier discharge plasma by adding CH4: scavenger chemistry at work, Sustain. Energy Fuels 3 (2019) 1388–1395.
[27] Z.Y. Yeo, T.L. Chew, P.W. Zhu, A.R. Mohamed, S.P. Chai, Conventional processes and membrane technology for carbon dioxide removal from natural gas: a review, J. Nat. Gas Chem. 21 (2012) 282–298.
[28] M. Aresta, A. Dibenedetto, A. Angelini, Catalysis for the valorization of exhaust carbon: from CO2 to chemicals, materials, and fuels. Technological use of CO2, Chem. Rev. 114 (2014) 1709–1742.
[29] T.P. Nunnally, K. Gutsol, R. A, A. Fridman, A.F. Gutsol, A. Kemoun, Dissociation of CO2 in a low current gliding arc plasmatron, J. Phys. D Appl. Phys. 44 (2011), 274009.
[30] M. Ramakers, G. Trenchev, S. Heijkers, W. Wang, A. Bogaerts, Gliding arc plasmatron: providing an alternative method for carbon dioxide conversion, ChemSusChem 10 (2017) 2642–2652.
[31] S. Van Alphen, F. Jardali, J. Creel, G. Trenchev, R. Snyders, A. Bogaerts, Sustainable gas conversion by gliding arc plasmas: a new modelling approach for reactor design improvement, Sustain. Energy Fuels 5 (2021) 1786–1800.
[32] F. Jardali, S. Van Alphen, J. Creel, H. Ahmadi Eshtehardi, M. Axelsson, R. Ingels, R. Snyders, A. Bogaerts, NOxproduction in a rotating gliding Arc plasma: potential avenue for sustainable nitrogen fixation, Green Chem. 23 (2021) 1748–1757.
[33] G. Trenchev, S. Kolev, W. Wang, M. Ramakers, A. Bogaerts, CO2 conversion in a gliding arc plasmatron: multidimensional modeling for improved efficiency, J. Phys. Chem. C 121 (2017) 24470–24479.
[34] G. Trenchev, A. Nikiforov, W. Wang, S. Kolev, A. Bogaerts, Atmospheric pressure glow discharge for CO2 conversion: model-based exploration of the optimum reactor configuration, Chem. Eng. J. 362 (2019) 830–841.
[35] G. Trenchev, A. Bogaerts, Dual-vortex plasmatron – a novel plasma source for CO2 conversion, J. CO2 Util. 39 (2020), 101152.
[36] S. Pancheshnyi, B. Eismann, G.J.M. Hagelaar, L.C. Pitchford, Computer Code ZDPlasKin, University of Toulouse, LAPLACE, CNRS-UPSINP, Toulouse, France, 2008. http://www.zdplaskin.laplace.univ-tlse.fr.
[37] G. Trenchev, S. Kolev, A. Bogaerts, A 3D model of a reverse Vortex flow gliding Arc reactor, Plasma Sources Sci. Technol. 25 (2016), 035014.
[38] H. Zhang, W. Wang, X. Li, L. Han, M. Yan, Y. Zhong, X. Tu, Plasma activation of methane for hydrogen production in a N2 rotating gliding arc warm plasma: a chemical kinetics study, Chem. Eng. J. 345 (2018) 67–78.
[39] S. Gröger, M. Ramakers, M. Hamme, J.A. Medrano, N. Bibinov, F. Gallucci, A. Bogaerts, P. Awakowicz, Characterization of a nitrogen gliding arc plasmatron using optical emission spectroscopy and high-speed camera, J. Phys. D Appl. Phys. (2019) 52.